ECS Journal of Solid State Science and Technology, 2021 10 041002
2162-8777/2021/10(4)/041002/9/$40.00 © 2021 The Electrochemical Society ("ECS"). Published on behalf of ECS by IOP Publishing Limited

Structural, Mechanical and Magnetic Characterization of Rare Earth Double Doped $SrBi_2Nb_2O_9$ lead Free Ceramics

Nagamani Sangula,[1] Nitchal Kiran Jaladi,[1,z] Siva Basivi Reddy Bhimavarapu,[2] Nageswara Rao Bhuvanagiri,[1] Anindhya Kiran Jaladi,[3] and Sambasiva Rao Konapala[4]

[1]*Division of Physics, Department of S&H, VFSTR deemed to be University, Guntur—522213, India*
[2]*Department of Mechanical Engineering, KHIT, Guntur—522019, India*
[3]*Department of Physics, Vignan Institute of Technology and Science, Hyderabad—508284, India*
[4]*Depatrment of Physics, Andhra University, Visakhapatnam—530003, India*

Lead free dielectric materials of Strontium Bismuth Niobate $SrBi_2Nb_2O_9$ (SBN) and rare earth double doped $SrBi_{1.8}Pr_{0.1}Gd_{0.1}Nb_2O_9$ (SBPGN), $SrBi_{1.8}Pr_{0.1}Y_{0.1}Nb_2O_9$ (SBPYN), $SrBi_{1.8}Eu_{0.1}Gd_{0.1}Nb_2O_9$ (SBEGN) and $SrBi_{1.8}Eu_{0.1}Y_{0.1}Nb_2O_9$ (SBEYN) were prepared by two-stage solid-state reaction route. The XRD studies have confirmed the formation of single-phase orthorhombic crystal structure. The microstructural analysis showed the formation of plausible needle shaped grains in the prepared ceramics. The FTIR study was used to investigate the effect of preparation and doping processes on the band intensities of the spectra. Mechanical studies showed that SBEGN and SBEYN ceramics exhibited mild wear ($<10^{-6}$ mm^3 Nm^{-1}) compared to others. The low friction coefficient values of SBPYN (0.044), SBEGN (0.058) and SBEYN (0.002) to that of SBN necessitate lattice strain in these materials. The VSM studies on the rare earth double doped SBN ceramic materials confirmed the induction and existence of magnetic order in SBPGN and SBEGN.
 [DOI: 10.1149/2162-8777/abf516]

Manuscript submitted February 15, 2021; revised manuscript received March 25, 2021. Published April 14, 2021.

Bismuth layered ferroelectric material $SrBi_2Nb_2O_9$ (SBN) is an Aurivillius compound and well established in 1949.[1,2] Bismuth layer structure Ferroelectric (BLSF) ceramics have been investigated because of their high Curie temperature (T_c), lower dielectric loss, excellent fatigue properties and short aging rates.[3–7] Among BLSFs, SBN has received special attention because it retains its structure even after doping compared to other Arivullius oxides of the bismuth layer.[8,9] SBN has a typical bismuth layer structure in which blocks of perovskite $(SrNb_2O_7)^{2-}$, made up of double octahedra of NbO_6 are interwoven with layers of $(Bi_2O_2)^{2+}$. Recently, many researchers have focused on the substitution of A and/or B sites in this ceramic system to enhance dielectric, ferroelectric and piezoelectric properties. They found that modification at site A is more effective than modification at site B in improving the ferroelectric and dielectric properties of BLSF ceramics.[10,11] Rare earth elements such as Nd^{3+}, La^{2+}, Gd^{3+}, Sm^{3+}, Pr^{3+}, Eu^{3+}, Ce^{3+} and Dy^{3+} have been introduced at $(Bi_2O_2)^{2+}$ layers of SBN by many researchers. The substitution at Bi^{3+} with Nd^{3+} increased the residual polarization, temperature coefficient of resonance frequency and piezoelectric constant.[12] It was observed that La^{3+} doping in bismuth layer of SBN ceramic resulted in pore free microstructure with low dielectric constant and high dielectric loss.[13] The Gd^{3+} substitution in SBN has lowered the Curie temperature (T_c) and dielectric constant and exhibited low dielectric loss. The random distribution of gadolinium between Bi_2O_2 layers has induced thermal behaviour in SBN.[14] In the case of SBN compounds doped with lanthanide, an increase in dielectric loss was observed due to the weight loss of bismuth during the sintering process.[15] The samarium or holmium substituted at bismuth has reduced the dielectric loss.[16,17] The red and green photoluminescence respectively has been noticed with either Eu^{3+} or Er^{3+}cations in SBN compound.[18,19] A decrease in the residual polarization and the coercive field was observed due to the substitution of Bi^{3+} ions by Pr^{3+} ions in $SrBi_{2-x}Pr_xNb_2O_9$ compounds (x = 0.2).[20] The SBN ceramics doped with Ce^{3+} exhibited higher Curie temperature and dielectric constant.[16] The Bi^{3+} ions replaced by Dy^{3+} ions have revealed the ferroelectric ordering in SBN.[21] DC conductivity, dielectric, impedance and modulus studies have been presented by double doping A-site with Potassium and Gadolinium in SBN by Ravi Kumar et al.[22,23] Barium and Gadolinium are simultaneously substituted at Strontium site of SBN by Sambasiva Rao et al., and found that T_c of SBN has increased from 392 °C–470 °C.[24] In view of the study of the above literature, it can be seen that few attempts have been made to study the structural, ferroelectric, dielectric and piezoelectric properties of rare earth double doping (simultaneous doping) at the Bi-site of SBN. For the first time, a valiant attempt has been made to investigate the effect of double doping on the structural, mechanical, and magnetic properties of lead-free BLSFs under solid-state reaction conditions. The novelty of this paper is that no researcher has quoted mechanical and magnetic properties of double doped rare earth SBN for checking their utility as wear-resistant tribo-materials and magnetic memory materials so far.

Experimental

Ceramic samples of $SrBi_2Nb_2O_9$ (SBN) and rare earth double doped $SrBi_{1.8}A_{0.1}B_{0.1}Nb_2O_9$ (where A = Pr/Eu; B = Gd/Y) were synthesized by a two-step solid-state reaction process. Powder with stoichiometric proportions, $SrCO_3$ (SRL, 98%), Bi_2O_3 (AVRA, 99%), Nb_2O_5 (AlfaBiochem, 99.9%), Pr_2O_3 (LobaChemie, 99.9%), Gd_2O_3 (SRL, 99.9%), Eu_2O_3 (SigmaAldrich, 99.99%) and Y_2O_3 (AVRA, 98%) were mixed and manually ground in an agate mortar for 8 h. and then calcined twice at 800°C for 2 h. A binder (polyvinyl alcohol) (PVA) is added to the heat-treated powder, and pellets having a diameter of 10 mm and a thickness of about 1 mm are made using a hydraulic press (7HPDEC427) at a pressure of 6 tons cm^{-2}. These pellets were sintered at 1120 °C for 2 h. The formation of grains in the samples was verified using XRD analysis (RigakuMiniflex 300/600) with CuKα radiation of wavelength 1.541A°. Lattice parameters and Cell volume are determined using POWD software and the prominent peaks were indexed. The morphology of the pellet samples was examined using SEM (vega3 tescan). The consequential shift in the band position in the rare earth double doped SBN materials compared to SBN has been analyzed from FTIR (YLS-QC-WQP-004) in the range of 4000–400 cm^{-1}. The mechanical properties, namely Vickers hard- ness (HV), coefficient of wear (K) and coefficient of friction (μ), were examined for the samples. The hardness was derived by the Vickers hardness tester under a load of 500 gm with a dwell time of 20 s. Wear and friction coefficient were found by using Pin on disc tribometer (Tribometer-201) under a load of 10 N and 575 revolutions per minute (rpm) with a dwell time of 12 min. The ferromagnetic properties of powders calcined at room temperature were

[z]E-mail: kiran.nischal@gmail.com

investigated using a vibrating sample magnetometer (VSM) (MicroSense-20130523-01).

Results and Discussion

X-ray Diffraction (XRD).—The X-ray diffractograms of the samples $SrBi_2Nb_2O_9$ (SBN), $SrBi_{1.8}Pr_{0.1}Gd_{0.1}Nb_2O_9$ (SBPGN), $SrBi_{1.8}Pr_{0.1}Y_{0.1}Nb_2O_9$ (SBPYN), $SrBi_{1.8}Eu_{0.1}Gd_{0.1}Nb_2O_9$ (SBEGN) and $SrBi_{1.8}Eu_{0.1}Y_{0.1}Nb_2O_9$ (SBEYN) are shown in the Fig. 1. The

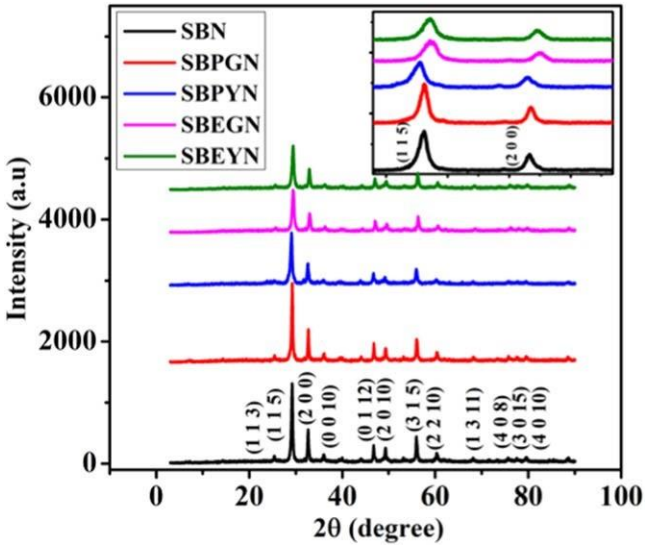

Figure 1. XRD patterns of SBN and $SrBi_{1.8}A_{0.1}B_{0.1}Nb_2O_9$ (A = Pr/Eu; B = Gd/Y) ceramic powders.

X-ray diffraction peaks obtained for SBN sample match the standard peaks of SBN and no extra peaks were observed. The highest peak (1 1 5) occurred is compatible with the (112 m+1) highest peak of diffraction in BLSF structures.[25] From Table I, a change in lattice parameter values of SBN was observed due to the introduction of rare earth double doped ions in the bulk of the crystal sample. The obtained ceramics are of single phase with orthorhombic structure. The average crystallite size was obtained from Debye–Scherrer formula by considering high intensity peak of (1 1 5). It is found that the crystallite size is decreased for the rare earth double doped SBN compared to SBN as given from Table II. The lattice strain for all the studied materials has been computed and is found to rise. The 2Θ value of prominent intensity peak (1 1 5) has been subjected to slight variation upon rare earth double doping in SBN materials, represented as inset figure in Fig. 1, indicating turn around in the structural distortion. Further, it may also be due to comparatively smaller ionic radius of dopant ion to that of Bi^{3+} ion. The observed peak broadening is indicative of structural disturbance in crystal due to lattice strain, caused due to introduction of dopants at $(Bi_2O_2)^{2+}$ layers of SBN. The POWD software was used to estimate Lattice parameters (a, b, c), Cell volume (V) and Orthorhombic distortion (b/a) of the samples and are given in Table I. The tolerance factor (t) values, given in Table II for all the studied materials reveal that the materials belong to Aurivillius family of ferroelectrics with perovskite structure.

Scanning electron microscopy analysis.—Figure 2a shows the plausible needle shaped grains present in the SBN sample. In the microscopic photographs of doubly doped rare earth SBN samples shown in Figs. 2b–2e, the grains are of unequal size and appear to be inhomogeneously distributed along with SBN. In addition, the microscopic image shows a porosity, which indicates that the sintering

Table I. Comparison of lattice parameters, orthorhombic distortion, cell volume on SBN and $SrBi_{1.8}A_{0.1}B_{0.1}Nb_2O_9$ (A = Pr/Eu; B = Gd/Y) of ceramics.

S. No	Composition	a (Aº)	b (Aº)	c (Aº)	Orthorhombic distortion(b/a)	Cell volume(Aº)
1.	SBN	5.5000	5.4600	25.0030	0.9927	750.84
2.	SBPGN	5.5070	5.5105	25.1418	1.0006	762.96
3.	SBPYN	5.5065	5.5130	25.0810	1.0011	761.39
4.	SBEGN	5.5065	5.5120	25.0840	1.0009	761.35
5.	SBEYN	5.5065	5.5235	25.0950	1.0030	763.27

Table II. Crystallite size, lattice strain and tolerance factor on SBN and $SrBi_{1.8}A_{0.1}B_{0.1}Nb_2O_9$ (A = Pr/Eu; B = Gd/Y) of ceramics.

S. No	Composition	Crystallite Size (nm)	Lattice Strain	Tolerance factor (t)
1.	SBN	28	0.0077	0.94
2.	SBPGN	25	0.0102	0.88
3.	SBPYN	18	0.0150	0.85
4.	SBEGN	19	0.0146	0.87
5.	SBEYN	21	0.0136	0.85

Table III. Investigated values of Grain size, % of density and porosity of SBN and $SrBi_{1.8}A_{0.1}B_{0.1}Nb_2O_9$ (A = Pr/Eu; B = Gd/Y) ceramic samples.

S. No	Composition	Grain size (μm)	% of Density	Porosity (%)
1.	SBN	1.99	94	0.0577
2.	SBPGN	1.34	95	0.0540
3.	SBPYN	5.68	95	0.0513
4.	SBEGN	5.33	95	0.0510
5.	SBEYN	2.20	95	0.0510

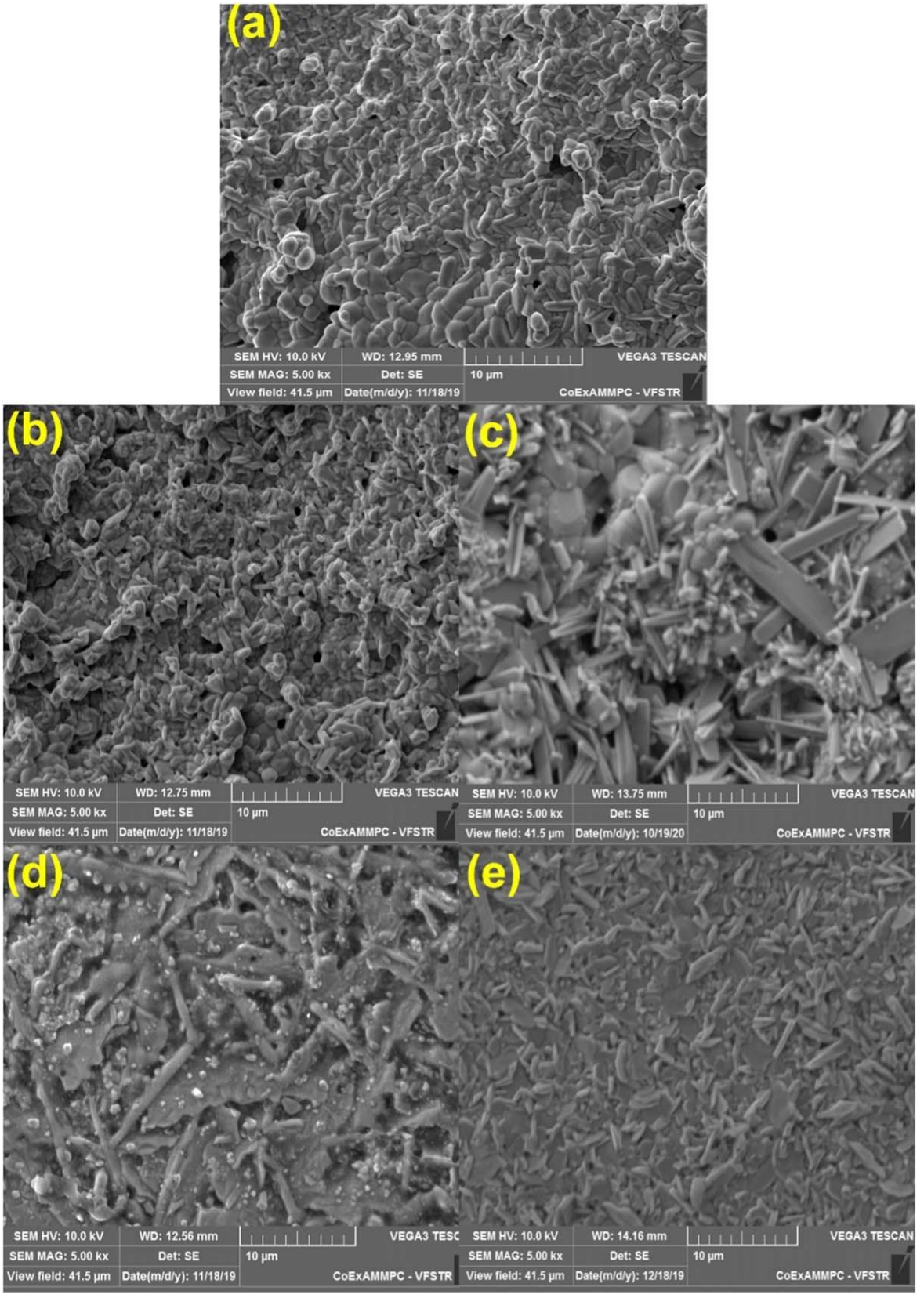

Figure 2. SEM micrographs of SBN and $SrBi_{1.8}A_{0.1}B_{0.1}Nb_2O_9$ (A = Pr/Eu; B = Gd/Y) gold coated ceramic samples.

conditions are optimal to obtain ceramics with high density.[26,27] The percentage of density was found to be in the range 94%–95% in all the ceramic samples, given in Table III. The average grain size was observed to vary and it is there to decrease in SBPGN and found to increase in SBPYN, SBEGN and SBEYN ceramic samples compared to SBN for the same sintering temperature, given in Table III. This

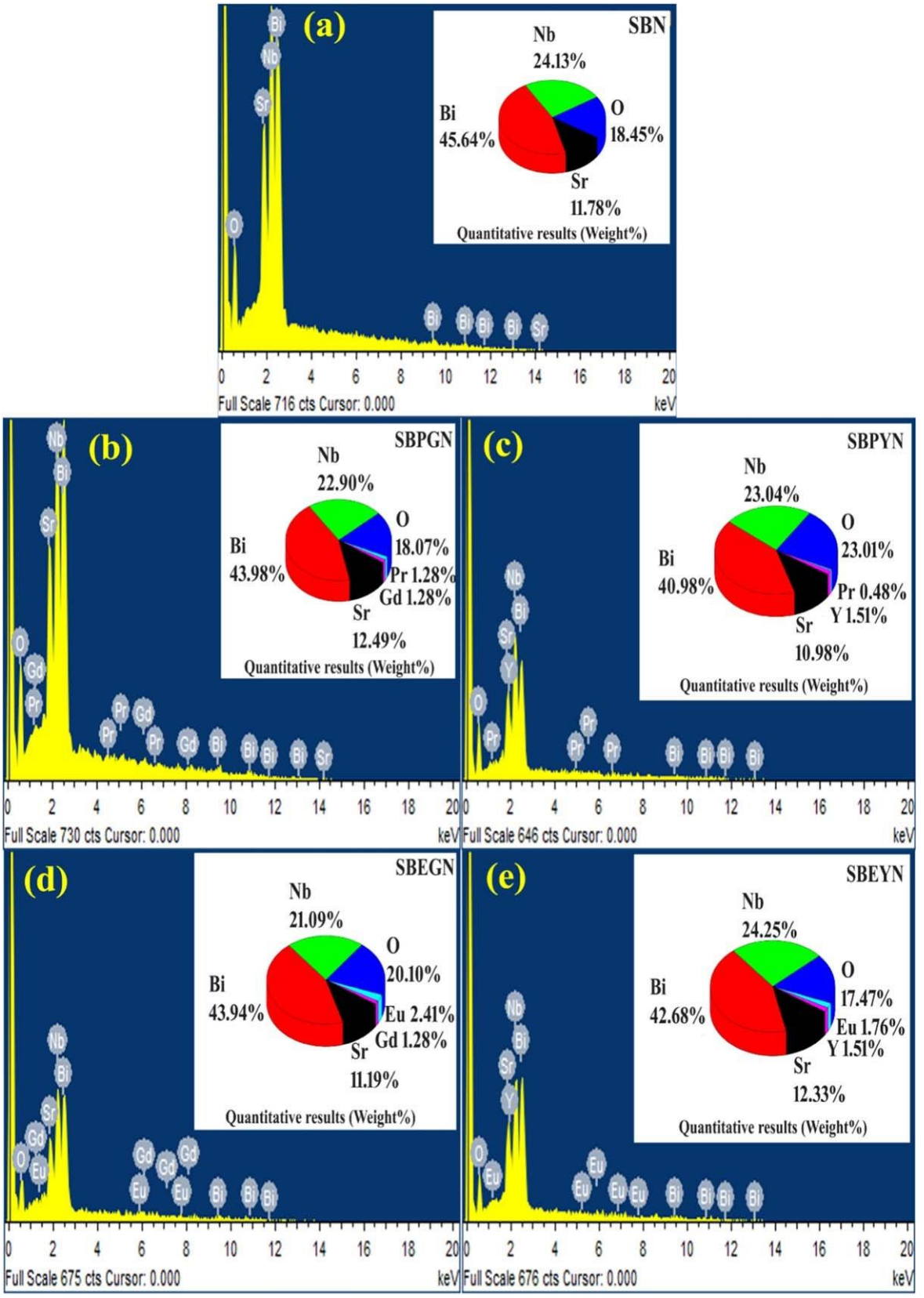

Figure 3. EDS spectra of $SrBi_{1.8}A_{0.1}B_{0.1}Nb_2O_9$(A = Pr/Eu; B = Gd/Y) ceramic compositions.

can be attributed to relatively smaller size impurity ions (Pr^{3+} and Gd^{3+}), which induce more kinking of the bond angle and a smaller tolerance factor that restricts the diffusion of rare earth ions, resulting in a smaller grain. The increased grain size may be due to agglomeration of particles and due to high volatilization of Bi ion in the process of sintering.

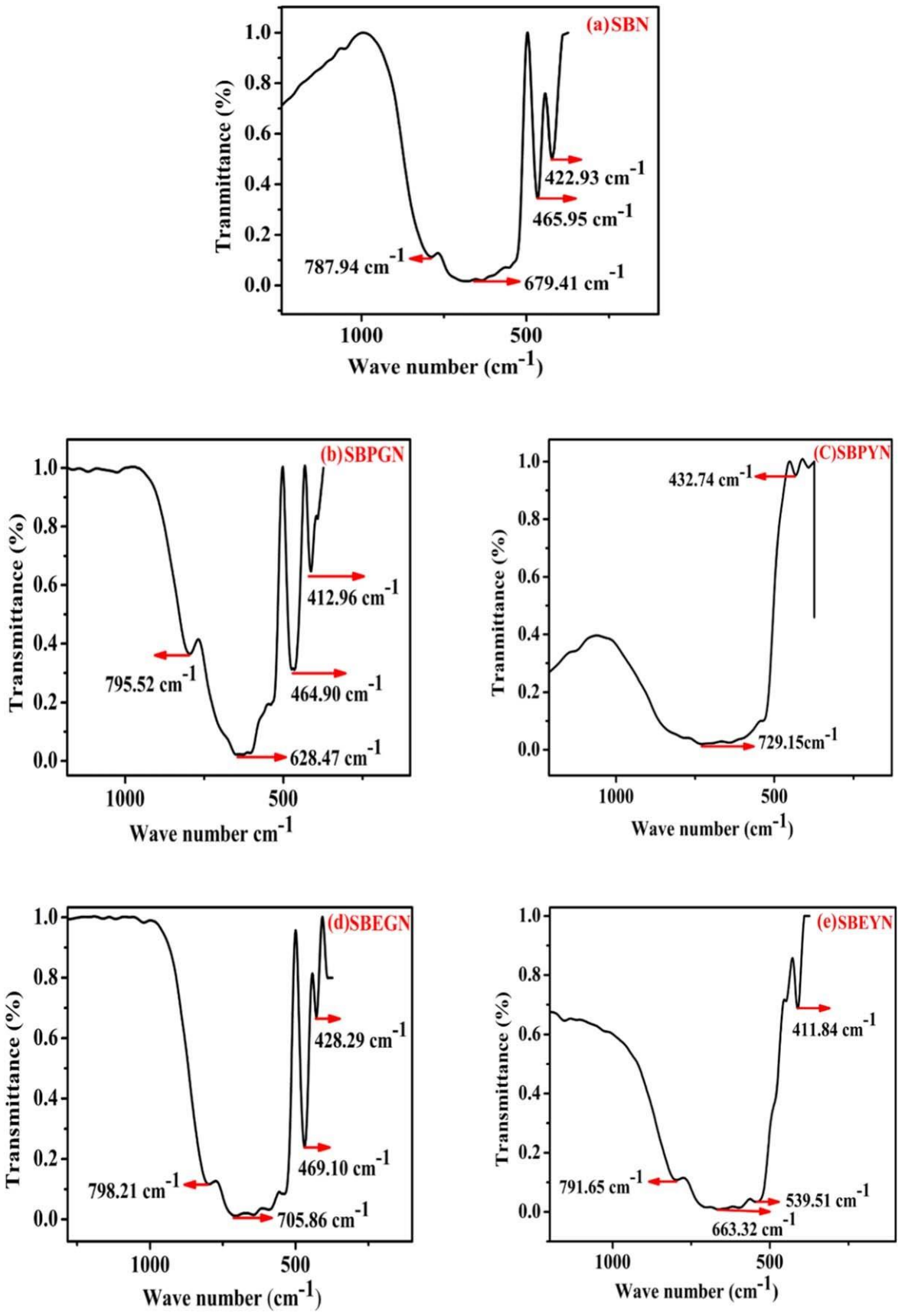

Figure 4. FTIR spectra of SBN and$SrBi_{1.8}A_{0.1}B_{0.1}Nb_2O_9$ (A= Pr/Eu; B = Gd/Y) ceramic compositions.

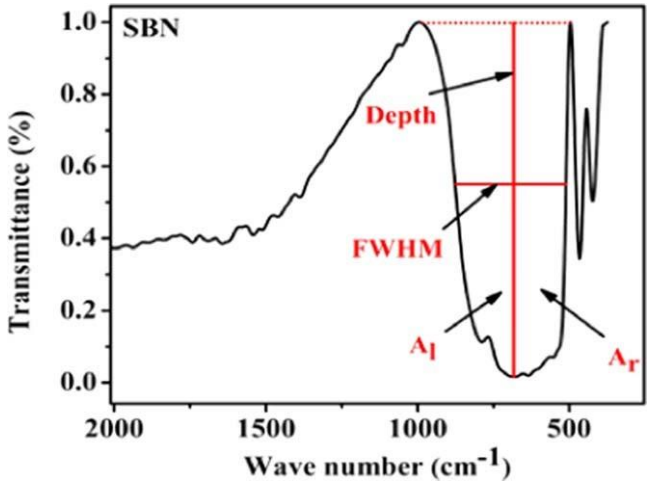

Figure 5. Definitions of the absorption feature of SBN.

Energy dispersive x-ray spectroscopy.—Figure 3 shows that the EDX Analysis of SBN and double doped SBN ceramics. The analysis primarily reveals that there are no impurities in the studied samples. SBN has elemental composition of Strontium, Bismuth, Niobium and Oxygen. The double doped samples as read from Figs. 3b–3e are induced with (Praseodymium, Gadolinium)/(Praseodymium, Yittrium)/(Europium, Gadolinium)/(Europium, Yittrium) respectively besides the elements of SBN constitution.

FTIR study.—Figure 4 shows that FTIR spectra of SBN and double doped rare earth ceramic materials (SBPGN, SBPYN, SBEGN and SBEYN). In the FTIR spectra of SBN shown in Fig. 4a, four absorption bands are found at 423 cm^{-1}, 466 cm^{-1}, 679 cm^{-1} and 788 cm^{-1} and they agree well with the data given.[28–30] The lower bands at 423 cm^{-1} and 466 cm^{-1} correspond to the NbO_6 bending vibration. The broad absorption band at around 679 cm^{-1} is due to the stretching vibration of NbO_6 and the band at 788 cm^{-1} has occurred from the Bi-O vibration of $(Bi_2O_3)^{2+}$ layers.[28,31] The bending vibrational bands are at 423 cm^{-1} and 466 cm^{-1} identified to shorter for SBPYN and sharper for SBPGN, SBEGN and SBEYN from SBN, indicating that the distortion of NbO_6 octahedra with rare earth double doping in SBN. The stretching vibration band (679 cm^{-1}) was found to be enlarged for SBPYN and SBEYN than the other samples of SBPGN and SBEGN. This may be due to the environment around the NbO_6 octahedron, to local structural changes due to the incorporation of foreign ions into the crystal structure. A slight change was observed for the absorption band at 788 cm^{-1} for the double doping of PG, EG, and EY at Bi-site of SBN and the same band was vanished for SBPYN. Thus, the absorption bands are identified to shifting towards lower wave number side for SBPGN, SBPYN and SBEYN, indicating that the interatomic force constant between Nb-O band is decreases with the sintering temperature,
Figs. 4b 4c and 4e. The shift observed in SBEGN towards higher wave number side may be ascribed to change in binding strength and atomic force constant due to heavier mass of Bi-atom compared to that of Eu and Gd, shown in Fig. 4d.[28,32–35]

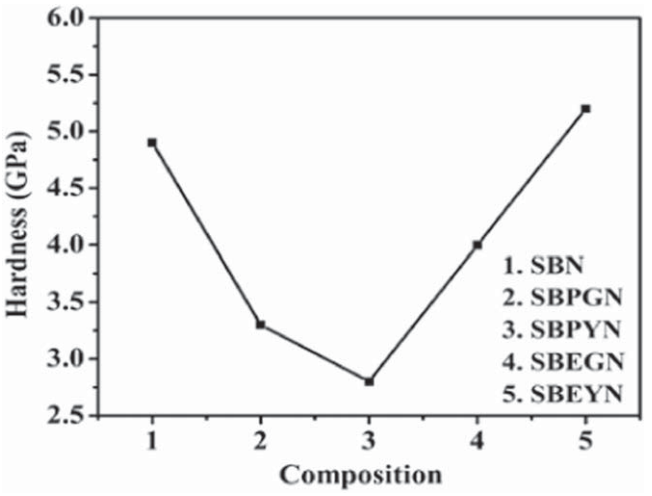

Figure 6. Variation of Vickers's hardness for SBN, SBPGN, SBPYN, SBEGN and SBEYN ceramic materials.

The full width at half maximum (FWHM) was defined as the width of the spectral elements at half maximum depth. The asymmetry factor was determined as follows:

$$s = \log (A_l/A_r) \quad [1]$$

Where A_l is the area to the left of the absorption position, and A_r is the area to the right of the point of maximum absorption to the end point.[36–38] The definition of absorption feature of SBN is given in Fig. 5. The results of the calculation such as position of the peak, asymmetry factor, relative depth, FWHM and crystallite size are summarized in Table IV. FTIR spectra of SBN, SBPGN and SBEYN enunciate that the area on the left-hand side is greater than the area on the right-hand side, such that the asymmetry values are positive for a skewed absorption features towards longer wavelength.[38] In SBPYN, the absorption feature has a perfect asymmetry, as the asymmetry factor is found to be zero. The area on the left-hand side has been found less than the area on the right-hand side for the ceramic sample SBEGN, the asymmetry value has been identified to be negative for a skewed absorption feature towards shorter wavelength.[37,39,40]

Mechanical studies.—In recent years, the use of ceramics as components in back-up systems has increased. Fundamental studies of hardness, coefficient of friction and coefficient of wear were carried out on ceramic materials SBN (BLSF) and double alloyed rare earths. This research mainly helps to understand the physical and chemical properties, as well as the behavior of materials in contact with themselves, other ceramic materials or metals. The purpose of this article is to review the above mechanical properties of the studied ceramic materials. Fig. 6 shows the variation of the digital Vickers micro hardness of the prepared ceramic materials obtained from the Eq. 2.

$$HV = 0.189\ F/D^2 GPa \quad [2]$$

Where "F" is the test force, "D" is the average of the diagonal length of the two indentations. Materials with good hardness can be used

Table IV. Data absorption feature characteristics of SBN, SBPGN, SBPYN, SBEGN and SBEYN from FTIR study.

Sample	Wave number (cm^{-1})	Asymmetry Factor	Relative depth (%)	FWHM (cm)	Crystallite size (nm)
SBN	692	0.36	1.37	694	28
SBPGN	627	0.30	1.47	1067	25
SBPYN	629	0.00	1.85	2623	18
SBEGN	706	−0.11	2.08	2895	19
SBEYN	664	0.22	2.00	2510	21

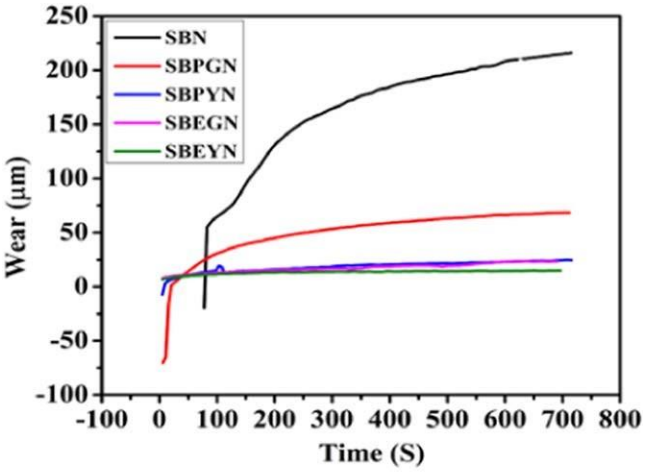

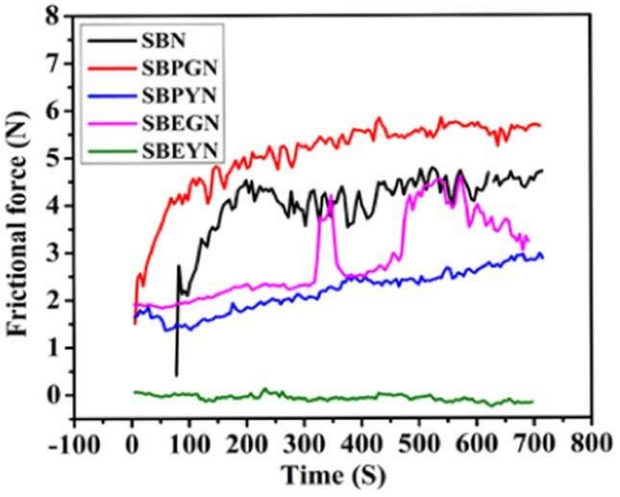

Figure 7. (a) Study of Wear for SBN, SBPGN, SBPYN, SBEGN and SBEYN ceramic specimens (b) Influence of frictional force on SBN and$SrBi_{1.8}A_{0.1}B_{0.1}Nb_2O_9$ (A= Pr/Eu; B = Gd/Y) ceramic specimens.

for applications requiring abrasion and corrosive wear resistance and they are suitable for ballpoint pen tips, bearings for precision instruments, cutting tool inserts, prosthetic hinge joints etc, The investigated material SBEYN has a good Vicker hardness (HV = 5.24 GPa).

In general, wear is classified as moderate to severe wear based on the ratio of the surface roughness (R_y) to the average grain size (D_g). Wear often occurs due to surface and subsurface defects and microcracks on the surface layers of contacting materials. The extent and distribution of such defects largely determines the size of the wear damage and the resulting wear particles. The above-mentioned features have been observed in SBN and $SrBi_{1.8}A_{0.1}B_{0.1}Nb_2O_9$ (A = Pr/Eu; B = Gd/Y) ceramics. The wear coefficient is calculated by the given Eq. 3 below.

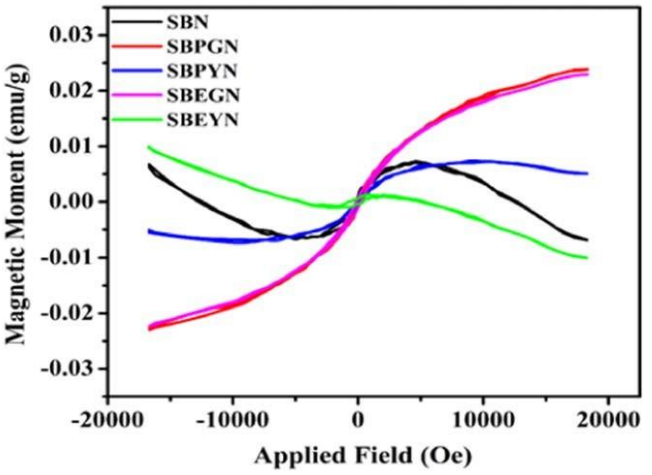

Figure 8. Magnetic hysteresis curve at room temperature by VSM for SBN and $SrBi_{1.8}A_{0.1}B_{0.1}Nb_2O_9$ (A = Pr/Eu; B = Gd/Y) ceramics compositions.

$$K = \frac{Wear\ volume}{Normal\ force * Sliding\ distance} \frac{mm^3}{N.m} \quad [3]$$

Figure 7a shows the wear in all studied samples with time. The wear rate obtained with (Ry/Dg > 0.5) is found to be less than 10^{-6} mm^3 Nm^{-1} in case of SBEGN and SBEYN exhibiting mild wear compared to other studied materials. This is indicative of a fact that the studied materials may be used as wear-resistant tribo- materials as compared to Polytetrafluoroethylene (PTFE).[40–42] The materials SBPGN and SBPYN have severe wear (>10^{-6} mm^3 Nm^{-1}) as that of the base material SBN, given in Table V. It is understood that inter granular fracture in all the studied ceramics was responsible for the removal of grains leading to severe wear. We also assume that pre—existing micro cracks at the grain boundary would have prompted micro-crack nucleation and hence severe wear.[43] This hypothesis and the wear model have been used by many researchers[44–51] to explain the transition mechanism in the mechan- ical wear of ceramics.

Figure 7b shows the effect of frictional force on SBN and $SrBi_{1.8}A_{0.1}B_{0.1}Nb_2O_9$ (A = Pr/Eu; B = Gd/Y) ceramic materials. The advanced structural ceramics have potential tribological applications.[51–53] The study of friction is mainly influenced by the crystallographic orientation and the presence of grain boundaries, which are crucial for understanding the process of friction in ceramics. Understanding tribo-chemical reactions will enable the selection and design of chemicals and lubricants specifically designed for ceramic tribological components. Friction coefficient is calculated by the given Eq. 4 below.

$$m = \frac{F_F}{F_N} \quad [4]$$

Where F_F is a tangential friction force in newton and F_N is the normal force in newton. The friction coefficient value has been

Table V. Study of vickers hardness, coefficient of wear and coefficient of friction for SBN and $SrBi_{1.8}A_{0.1}B_{0.1}Nb_2O_9$ (A = Pr/Eu; B = Gd/Y) ceramic materials.

S.No	Composition	Vickers Hardness (HV) (GPa)	Coefficient of Wear (K) (mm^3 $N.m^{-1}$)	Coefficient of friction (μ)
1.	SBN	4.9	1.9×10^{-4}	0.102
2.	SBPGN	3.3	1.2×10^{-4}	0.083
3.	SBPYN	2.8	2.8×10^{-5}	0.044
4.	SBEGN	4.0	8.4×10^{-6}	0.058
5.	SBEYN	5.2	1.6×10^{-6}	0.002

Table VI. Magnetization values of SBN and rare earth double doped (SBPGN, SBPYN, SBEGN and SBEYN) ceramic materials.

S. No	Composition	M_{sat} (emu g^{-1})	M_{rem} (emu g^{-1})	H_c (Oe)
1.	SBN	0.007	0.0003	0
2.	SBPGN	0.024	0.0005	125
3.	SBPYN	0.007	0.002	150
4.	SBEGN	0.022	0.0006	169
5.	SBEYN	0.010	0.0003	0

identified to be low in case of rare earth double doped ceramic samples namely SBPYN (0.044), SBEGN (0.058) and SBEYN (0.002) when compared to SBN (0.102). It is found to be 0.083 in case of SBPGN ceramic, given in Table V. In addition, ceramics with a low coefficient of friction allow the implementation of tribological components that can operate in dry conditions or in environments with poor lubrication, since they have self-lubricating properties, which leads to increased service life and reduced maintenance costs.[54] The studied materials of SBPYN SBEGN and SBEYN may exhibit self-lubricating property owing to their low frictional coefficient values as that of PTFE.[41,42]

Vibrating Sample Magnetometer (VSM).—In the recent past, dopant mediated ferromagnetic hybridization was discussed by different research groups.[55] The room temperature magnetization behavior of SBN and $SrBi_{1.8}A_{0.1}B_{0.1}Nb_2O_9$ (A = Pr/Eu; B = Gd/Y) were shown in Fig. 8. From the M-H plots, it is clear that pure SBN, SBPYN and SPEYN ceramic species exhibit the diamagnetic nature which may be an indication of absence of magnetic domains. The appearance of M-H hysteresis loop confirms the induction and existence of magnetic order in the studied ceramic materials of SBPGN and SBEGN as shown in Fig. 8. This may be due to incorporation of rare earth ions of Pr/Gd and Eu/Gd at Bi- site of SBN lattice, which might have suppressed the diamagnetic signature. This can also be attributed to localized f-states of RE dopants and due to interaction between conduction electrons and 4f shell electrons (s-f interaction).[56–59] The obtained values of coercivity (H_c), Saturation magnetization (M_s) and Remnant magnetization (M_r) of all the studied materials are given in Table VI. Ferromagnetic hysteresis loops could arise due to the ferromagnetic interaction of Pr^{3+}/Gd^{3+} and Eu^{3+}/Gd^{3+} ions, which completely diffused into the SBN host matrix. In addition, some anionic defects such as oxygen vacancies (V_O) would be created to maintain charge neutrality upon doping in terms of defect magnetism. Each oxygen vacancy (V_O) serves as an electron gap. An F-center is created when an electron gets trapped at oxygen vacancy.[60] An increase in the magnetization value could be due to rare earth double doping at Bi-site of SBN material as it might have set in ferromagnetic ordering.[61] The observed phenomena can also be attributed to the formation of super exchange interaction between dopant ions which are close to each other.[62] Moreover, the interaction of magnetic ions with parent material will also decide magnetic properties.[63] From the above, it is understood that ferromagnetic ordering in the studied ceramic materials might have been due to rare earth ion double doping at Bi-site of SBN, which leads to oxygen vacancies (Vo), the formation of F- centers, and a change in the morphology and particle size. The hysteresis loops at the higher fields (greater than 10Koe) become linear for SBPGN and SBEGN ceramic composition. This may be due to antiparallel spin clusters or cantered nature of spin in antiferromagnetic materials, which are gradually turned towards the field direction giving rise to ferroelectric nature of the materials SBPGN and SBEGN.[64] The low area hysteresis loop shows that the materials studied are of soft magnetic nature.[65]

Conclusions

This work focused on the solid-state synthesis and characterization of SBN ceramic materials and double-doped rare earths. X-ray diffraction studies confirmed the formation of a single-phase orthorhombic crystal structure in all calcined powders. SEM micrographs revealed the grains are of unequal size and appear to be inhomogeneously distributed in all studied samples with the inhibition of porosity. The characteristics of FTIR spectra illustrated the effect of rare earth ion double doping at Bi-site of SBN and the asymmetry of absorption was determined for all the studied samples. Mechanical properties of Hardness, Wear and Friction coefficients have been obtained on SBN and rare earth double doped SBN ceramic materials. Good mechanical properties were exhibited by SBEGN and SBEYN ceramic compositions over the other studied samples, basing on which the materials may find applications as wear resistant tribo-materials and may be potentially utilized as self-lubricating ceramic composites. The zero coercivity of SBN and SBEYN ceramics indicates the absence of magnetic domains. The occurrence of M-H hysteresis loops confirms the induction and existence of magnetic order in the studied ceramic materials of SBPGN and SBEGN. The low area hysteresis curves of SBPGN and SBEGN ceramic species establish that the materials are of soft magnetic in nature.

Acknowledgments

The authors would like to thank VFSTR, deemed to be University, Guntur for financial support for this research work, and CoExAMMPC for providing key characterizations.

ORCID

Nitchal Kiran Jaladi https://orcid.org/0000-0002-6585-6067

References

1. D. P. Volanti, L. S. Cavalcante, E. C. Paris, A. Z. Simões, D. Keyson, V. M. Longo, A. T. de Figueiredo, E. Longo, and J. A. Varela, *Appl. Phys. Lett.*, 90, 261913 (2007).
2. K. Watanabe, M. Tanaka, E. Sumitomo, K. Katori, H. Yagi, and J. F. Scott, *Appl. Phys. Lett.*, 73, 126 (1998).
3. Z. Yao, R. Chu, Z. Xu, J. Hao, D. Wei, and G. Li, *J. Mater. Sci.: Mater. Electron.*, 26, 8740 (2015).
4. X. Meng, W. Ma, Q. Li, J. Ma, B. Niu, and N. Chen, *J. Mater. Sci.: Mater. Electron.*, 25, 4585 (2014).
5. T. Wei, C. P. Li, Q. J. Zhou, Y. L. Zou, and L. S. Zhang, *Mater. Lett.*, 118, 92 (2014).
6. Y. Liu, Y. Lu, and S. Dai, *J. Alloys Compd.*, 484, 801 (2009).
7. Z. G. Yi, Y. X. Li, Q. B. Yang, and Q. R. Yin, *Ceram. Int.*, 34, 735 (2008).
8. N. Pavlović, V. Koval, J. Dusza, and V. V. Srdić, *Ceram. Int.*, 37, 487 (2011).
9. H. Naceur, A. Megriche, and M. El Maaoui, *J. Alloys Compd.*, 546, 145 (2013).
10. P. Fang, Z. Xi, W. Long, X. Li, and J. Li, *J. Alloys Compd.* (2013).
11. C.-M. Wang, S. Zhang, J.-F. Wang, M.-L. Zhao, and C.-L. Wang, *Mater. Chem. Phys.*, 118, 21 (2009).
12. L. Sun, J. Chu, P. Yang, F. Yue, Y. Li, C. Feng, and C. Mao, *Trans. Nonferrous Met. Soc. China*, 19, 1459 (2009).
13. V. Shrivastava, A. K. Jha, and R. G. Mendiratta, *Physica B*, 371, 337 (2006).
14. M. Afqir, A. Tachafine, D. Fasquelle, M. Elaatmani, A. Zegzouti, J. C. Carru, and M. Daoud, *J. Mater. Sci.: Mater. Electron.*, 29, 1289 (2018).
15. M. Afqir, A. Tachafine, D. Fasquelle, M. Elaatmani, J.-C. Carru, A. Zegzouti, and M. Daoud, *Solid State Sci.*, 73, 51 (2017).
16. M. Afqir, A. Tachafine, D. Fasquelle, M. Elaatmani, A. Zegzouti, J. C. Carru, and M. Daoud, *Moscow Univ. Phys. Bull.*, 72, 196 (2017).
17. M. Afqir, A. Tachafine, D. Fasquelle, M. Elaatmani, J.-C. Carru, A. Zegzouti, and M. Daoud, *Sci. China Mater.*, 59, 921 (2016).
18. T. Wei, C. Z. Zhao, Q. J. Zhou, Z. P. Li, Y. Q. Wang, and L. S. Zhang, *Opt. Mater. (Amst).*, 36, 1209 (2014).
19. D. P. Volanti, I. L. V. Rosa, E. C. Paris, C. A. Paskocimas, P. S. Pizani, J. A. Varela, and E. Longo, *Opt. Mater. (Amst).*, 31, 995 (2009).
20. S. Huang, C. Feng, L. Chen, and X. Wen, *Solid State Commun.*, 133, 375 (2005).
21. A. Srinivas, F. Y. C. Boey, and T. Sritharan, *J. Electroceramics.*, 16, 321 (2006).
22. B. Ravi Kumar, N. V. Prasad, G. Prasad, and G. S. Kumar, *Materials Today: proceeding.*, 11, 1036 (2019).
23. B. Ravi Kumar, N. Venkata Prasad, G. Prasad, and G. Subramanyam Kumar, *Trans. Ind. Ceram. Soc.*, 78, 89 (2019).
24. K. SambasivaRao, D. Madhava Prasad, P. Murali Krishna, B. Hima Bindu, and K. Suneetha, *J. Mater. Sci.*, 42, 7363 (2007).
25. C. L. Diao, J. B. Xu, H. W. Zheng, L. Fang, Y. Z. Gu, and W. F. Zhang, *Ceram. Int.*, 39, 6991 (2013).
26. M. Afqir, A. Tachafine, D. Fasquelle, M. Elaatmani, J.-C. Carru, A. Zegzouti, and M. El Hammioui, *Int. J. Miner. Metall. Mater.*, 25, 1304 (2018).
27. D. Dhak, P. Dhak, and P. Pramanik, *Appl. Surf. Sci.*, 254, 3078 (2008).
28. M. Verma, A. Tanwar, K. Sreenivas, and V. Gupta, *Ferroelectrics*, 404, 233 (2010).
29. A. Tanwar, K. Sreenivas, and V. Gupta, *J. Appl. Phys.*, 105, 084105 (2009).

30. S. Kumar, M. Panneerselvam, P. Vinatier, and K. J. Rao, *Ferroelectrics*, 306, 165 (2004).
31. J. Nitchal Kiran, M. Sreenivasulu, K. Sambasiva Rao, K. Srinivasa Rao, S. Nagamani, and T. Nagamalleswari, *Material Today Proceedings.*, 19, 2658 (2019).
32. Y. X. Li, G. Chen, H. J. Zhang, Z. H. Li, and J. X. Sun, *J. Solid State Chem.*, 181, 2653 (2008).
33. M. Zhu, L. Sun, W. W. Li, W. L. Yu, Y. W. Li, Z. G. Hu, and J. H. Chu, *Mater. Res. Bull.*, 45, 1654 (2010).
34. J. T. Last, *Phys. Rev.*, 105, 1740 (1957).
35. M. Afqir, A. Tachafine, D. Fasquelle, M. Elaatmani, J.-C. Carru, A. Zegzouti, and M. Daoud, *Chin. J. Phys.*, 56, 1158 (2018).
36. F. van der Meer, *Int. J. Appl. Earth Obs. Geoinf.*, 5, 55 (2004).
37. N. Zaini, F. van der Meer, and H. van der Werff, *Remote Sens.*, 4, 987 (2012).
38. J. W. Hopkin, K. S. Seshadri, N. B. W. Jonathan, and J. W. Hopkins, *Can. J. Chem.*, 41, 750 (1963).
39. F. A. Kruse, A. B. Lefkoff, and J. B. Dietz, "Expert system-based mineral mapping in Northern Death-Valley, California Nevada, using the airborne visible infrared imaging spectrometer (AVIRIS)." *Remote Sens. Environ.*, 44, 309 (1993).
40. K. Adachi, K. Kato, and N. Chen, *Wear*, 203–204, 209 (1997).
41. G. Suresh, V. Vasu, and M. V. Rao, *Silicon*, 10, 2043 (2018).
42. Y. Şahin, *Cogent Eng*, 2, 1000510 (2015).
43. H. P. Krichner and R. M. Gruver, *J. Am. Ceram.*, 53, 232 (1970).
44. K. Hokkiriigawa and K. Kato, "Wear mode diagram of ceramics." *Proc., 33rd JSLE Conf.*, 9 (1989).
45. K. Hokkiriigawa, *Wear*, 151, 219 (1991).
46. H. Kong and M. F. Ashby, *Acta Metall.*, 40, 2907 (1992).
47. S. J. Cho, B. J. Hockey, B. R. Lawn, and S. J. Bennison, *J. Am. Ceram, Soc.*, 72, 1249 (1989).
48. S. Jahanmir and X. Dong, *Trans. ASME, J. Tribol.*, 28, 1 (1991).
49. Y. S. Wang, S. M. Hsu, and R. G. Munro, "A wear model for alumina sliding wear." *Proc, Japan Int. Tribology Conf. Nagoya*, 1225 (1990).
50. S. S. Kim, S. W. Kim, and S. M. Hsu, "A new parameter for assessment of ceramic wear." *Proc, 6th Nordic symp. On Tribology, Nordtrib.*, 94, 485 (1994).
51. H. D. Buckley and kazuhisa Miyoshi, *Wear*, 100, 333 (1984).
52. K. Miyoshi and D. H. Buckley, *ASLE Tmns.*, 22, 79 (1979).
53. K. Miyoshi and D. H. Buckley, *Am. Ceram. Sot. Bull.*, 62, 494 (1983).
54. G. Straffelini, "Friction." *Friction and Wear Methodologies for Design and Control* (Springer, Switzerland) Springer Tracks Mechanical Engineering, 1st ed., 21 (2015).
55. M. Avinash, M. Muralidharan, and K. Sivaji, *Physica B Condens. Matter*, 570, 157 (2019).
56. Samuel Hsi and Peh Liu, *Magnetic Properties of Rare Earth Metals* (Iowa State University, Iowa, United States) 1 (1960).
57. G. S. Anderson and S. Legvold, *Phys. Rev. Lett.*, 1, 322 (1958).
58. R. Brout and H. Suhl, *Phys. Rev. Lett.*, 2, 387 (1959).
59. H. Suhl and B. T. Matthias, *Phys. Rev.*, 114, 977 (1959).
60. K. Balamurugan, N. Harish Kumar, B. Ramachandran, and M. S. RamachandraRao, *Solid State Commn.*, 149, 884 (2009).
61. K. Upendra, *Mater. Res. Express*, 4, 11 (2017).
62. K. Subramanyam, N. Sreelekha, G. Murali, D. Amaranatha Reddy, and R. P. Vijayalakshmi, *Physica B*, 454, 86 (2014).
63. B. Choudhury and A. Choudhury, *J. Appl. Phys.*, 114, 203906 (2013).
64. S. K. PatriBibhuti and B. Sahu, *Ferroelectrics*, 518, 178 (2017).
65. E. Irfan, Z. Rabab, M. Kiran, J. Arifa, and A. Nasir, *Afr. J. Pure Appl. Chem.*, 6, 1 (2012).